High-performance hybrid biofuel cells using amphiphilic assembly based enzyme electrodes Ⓕ

ⒾⒹ Cheong Hoon Kwon, ⒾⒹ Minchul Kang, ⒾⒹ Minseong Kwon, et al.

COLLECTIONS

Ⓕ This paper was selected as Featured

View Online   Export Citation   CrossMark

High-performance hybrid biofuel cells using amphiphilic assembly based enzyme electrodes Ⓕ

View Online   Export Citation   CrossMark

Cheong Hoon Kwon,[1] ⓘD Minchul Kang,[1] ⓘD Minseong Kwon,[1] ⓘD Donghyeon Nam,[1] ⓘD Yongkwon Song,[1] Euiju Yong,[1] Min-Kyu Oh,[1] Yongju Kim,[2] Bongjun Yeom,[3] Jun Hyuk Moon,[4] Seung Woo Lee,[5,a] ⓘD and Jinhan Cho[1,2,a] ⓘD

AFFILIATIONS

[1] Department of Chemical & Biological Engineering, Korea University, 145 Anam-ro, Seongbuk-gu, Seoul 02841, Republic of Korea
[2] KU-KIST Graduate School of Converging Science and Technology, Korea University, 145 Anam-ro, Seongbuk-gu, Seoul 02841, Republic of Korea
[3] Department of Chemical Engineering, Hanyang University, 222 Wangsimni-ro, Seongdong-gu, Seoul 04763, Republic of Korea
[4] Department of Chemical and Biomolecular Engineering, Sogang University, Baekbeom-ro 35, Mapo-gu, Seoul 04107, Republic of Korea
[5] The George W. Woodruff School of Mechanical Engineering, Georgia Institute of Technology, Atlanta, Georgia 30332, USA

[a] Authors to whom correspondence should be addressed: seung.lee@me.gatech.edu and jinhan71@korea.ac.kr

ABSTRACT

Biofuel cells, which convert chemical energy into electrical energy at mild temperature and over moderate pH ranges, have been considered some of the most promising candidates for powering biomedical devices. However, most biofuel cells provide low power output and short-term operational stability due to their poor electron transfer. To address these issues, we use a unique amphiphilic assembly method to generate hybrid biofuel cells with high power output and good operational stability. This approach can induce favorable interfacial interactions between electrocatalysts and significantly improve the electron transfer kinetics of electrodes. In this study, glucose oxidase (in aqueous media) is repeatedly assembled with hydrophobic metal nanoparticles (in nonpolar media) on a conductive textile. The formed biofuel cell exhibits remarkably high power output (7.3 mW cm^{-2}) and good operational durability. We believe that our assembly approach can provide a basis for preparing a variety of high-performance bioelectrochemical devices, including biofuel cells.

Published under an exclusive license by AIP Publishing. https://doi.org/10.1063/5.0084917

I. INTRODUCTION

Enzyme electrodes have long been widely used in various applications, including biosensing systems and electrochemical devices.[1,2] In particular, biofuel cells (BFCs), which can convert biochemical energy into electricity under mild biological conditions, are particularly promising candidates for powering a variety of bioelectronic devices.[3,4] However, despite the promising characteristics of BFCs, their low power output has remained a critical drawback over the last few decades.[5] To address this problem, many research efforts have focused on enhancing electron transfer at enzyme/host electrodes and enzyme/enzyme interfaces and developing more effective enzyme immobilization methods.

First, the incorporation of redox mediators into BFC electrodes [i.e., mediated electron transfer-based BFC (MET-BFC) electrodes] has been most widely used for improving electron transfer within electrodes.[5–8] However, because of problematic issues such as the biological toxicity, instability, and complicated synthesis of many redox

mediators, recent studies have paid a great deal of attention to increasing the electron transfer and power output in direct electron transfer-based BFCs (DET-BFCs) without redox mediators.[7] Although the power outputs of most DET-BFCs (a few to tens of μW cm^{-2}) are much inferior to those of MET-BFCs (tens to hundreds of μW cm^{-2}), the power outputs of the DET-BFCs have been gradually enhanced through various challenging approaches for improving electron transfer between enzymes and electrodes.[9,10] For example, it was reported by Cosnier group that the power output of carbon nanotubes (CNTs) support-based DET-BFC using solution drop casting and high mechanical compression could be increased up to 1.25 mW cm^{-2}.[11] Additionally, Kano group reported that DET-BFC composed of fructose dehydrogenase (for anode) and multi-copper oxidase (for cathode) were prepared onto carbon cryogel, which exhibited the maximum power density of 2.6 mW cm^{-2}.[12]

A notable approach to realizing effective electron transfer is an electron relay effect achieved by embedding metal nanoparticles (NPs)

among enzymes.[13–15] In most cases, the integration of charged metal NPs with enzymes in water has been accomplished using reconstitution, physical adsorption, and/or blending methods. Furthermore, a variety of conductive carbon-based nanomaterials [i.e., carbon nanotubes (CNTs), graphene, reduced graphene oxide (rGO), and nitrogen-doped graphite carbon nitride nanosheets] have also been used to increase the active surface area of electrodes as well as to decrease the distances between active sites (buried about 15 Å below the protein surface) and electrodes.[16–19] Although the conductive materials with high surface-to-volume ratios are randomly distributed in the conductive matrix, they can provide the opportunity for favorable enzyme wiring for DET.[2,20] However, these approaches impose limitations on further improving electron transfer due to the use of inactive organics (including crosslinkable polymers), the low packing density of electrostatically charged metal NPs or enzymes (by electrostatic repulsion in water), and the intrinsically low electrical conductivity of carbon-based materials.[11,21–24] Additionally, these enzyme electrodes suffer from enzyme instability, ineffective immobilization, and slow electron transport between catalytic active sites.[25] For overcoming these issues related to the DET of Gox in some degree, a few research groups have used porous conductive support or layer-by-layer (LbL) assembly approach.[2,26,27] However, the effective electron transfer between neighboring enzymes has still remained a critical issue.

Furthermore, little experimental consensus exists on the optimal thickness, although increasing the thickness eventually suppresses the electron transfer efficiency of the enzyme layer. Specifically, in the case of using conventional methods for immobilizing glucose oxidase (GOx) on electrodes, the thicknesses of GOx composite films have been widely distributed from tens of nanometers (nm) (produced by the electrostatically charged Au NP–reconstitution method) to a few micrometers (μm) (produced by mechanical pressing).[11] Additionally, these methods still have considerable difficulty in realizing the architecture of regular thin films with a high density of GOx and producing robust electrodes for effective electron transfer, high power output, and long-term operation.

Herein, we introduce an amphiphilic assembly based enzyme fibril electrode with facile electron transfer, an exceptionally high power output ($\sim$7.3 mW cm^{-2}), and good operational stability. Our amphiphilic assembly process, which is based on the high affinity between enzyme amino acids (in aqueous solvent) and the surface of hydrophobic metal (or metal oxide) NPs (in a nonpolar solvent), forms nanoblended GOx/hydrophobic NP films with unprecedently high electron transfer on metallic textiles or fibers (Fig. 1). Particularly, our DET-BFC electrode possesses both the macroporous (by the use of fibril-based textile) and nanoporous (by the formation of nanovoids between neighboring Au NPs) structure by depositing the LbL-assembled (GOx/Au NPs)$_n$ multilayers onto the highly porous fibril textile electrode. Additionally, we highlight that our amphiphilic assembly-based LbL combination of GOx and conductive Au NPs can provide highly uniform nano-confined structure and conformal coating in nano-scale, which can effectively decrease the electron transfer distance between GOx and Au NPs (Fig. S1 in the supplementary material). These findings also suggest that various biomaterials, including enzymes, can be easily and directly combined with a variety of hydrophobic and conductive NPs with desirable functionalities. In particular, our approach can generate the direct contact between NPs

and enzymes without unnecessary insulating organics (i.e., organic ligands or linkers bound to the surface of NPs) as well as the high packing density of conductive NPs (by the use of hydrophobic NPs that do not electrostatically repel each other) on the enzyme layer, which leads to a strong electron relay effect within the ultrathin nanocomposite film ($\sim$30 nm thickness). Owing to these notable characteristics, the electron transfer between the enzyme and host electrode (by favorable interfacial interaction and conformal coating) and between neighboring enzymes (by an electron relay effect) can be significantly enhanced, which can also increase the power output of BFCs. Although in our study, various ultrathin GOx-assembled films using cationic small molecule linkers and/or anionic metal NPs could also enhance the electron transfer within GOx-based electrodes, these obtained power outputs are still inferior to the performance of GOx films formed by the amphiphilic assembly.

The assembled 3D porous textile- and fiber-based hybrid BFCs exhibit high power outputs (1.5 mW cm^{-2} for textile BFCs and 7.3 mW cm^{-2} for fiber BFCs) without using redox mediators, which outperforms the power outputs of reported DET- and MET-BFCs thus far. Additionally, our BFC electrodes, which are measured in an electrolyte environment similar to physiological conditions, also maintain approximately 81% and 61% of the initial power density even after continuous operation for 20 and 60 days, respectively, demonstrating their good operational stability. Considering that amphiphilic assembly can efficiently control electron transfer within electrodes, we believe that our strategy can provide a basis for developing a variety of high-performance electrochemical applications beyond BFCs.

II. RESULTS AND DISCUSSION
A. Preparation of metallic cotton textile-based host electrodes

To prepare host electrodes for cotton textile or fiber-based BFCs, we used a layer-by-layer (LbL) assembly approach based on the complementary interactions between two different components in organic/organic media.[17,23,24,28,29] First, we investigated the adsorption behavior of tetraoctylammonium bromide (TOA)-stabilized Au NPs (TOA-Au$_{NPs}$) and diethylenetriamine (DETA) linkers onto substrates.[30] Particularly, it was anticipated that DETA (M$_w$ $\approx$103 g mol^{-1}), as an extremely small molecular linker, could minimize the separation distance between neighboring Au$_{NPs}$ compared to other organic linkers, such as amine-functionalized polymers or tris(2-aminoethyl)amine (M$_w$ $\approx$146 g mol^{-1}). TOA-Au$_{NPs}$ were LbL-assembled with DETA onto a poly(ethylene imine) (PEI)-coated Si wafer (Fig. S2 in the supplementary material). While conventional LbL assemblies employ electrostatic and/or hydrogen-bonding interactions in aqueous media,[28,29] this LbL approach is based on the high affinity (i.e., coordination-bonding interaction) between amine groups and metal (or metal oxide) surfaces in organic/organic media.[17,20–23,31] During repeated LbL deposition, small DETA linkers adsorbed onto the surfaces of Au$_{NPs}$ via a ligand exchange reaction with the bulky TOA ligands (M$_w$ $\approx$322 g mol^{-1}) since the NH$_2$ groups of the DETA linkers had a high affinity for Au$_{NPs}$; this behavior was confirmed by Fourier transform infrared (FTIR) spectroscopy (Fig. S3 in the supplementary material). This ligand exchange reaction-based LbL assembly of TOA-Au$_{NPs}$ and DETA was further verified by quartz crystal microbalance (QCM) analysis and UV-vis spectroscopy (Figs. S4 and S5 in the supplementary material).
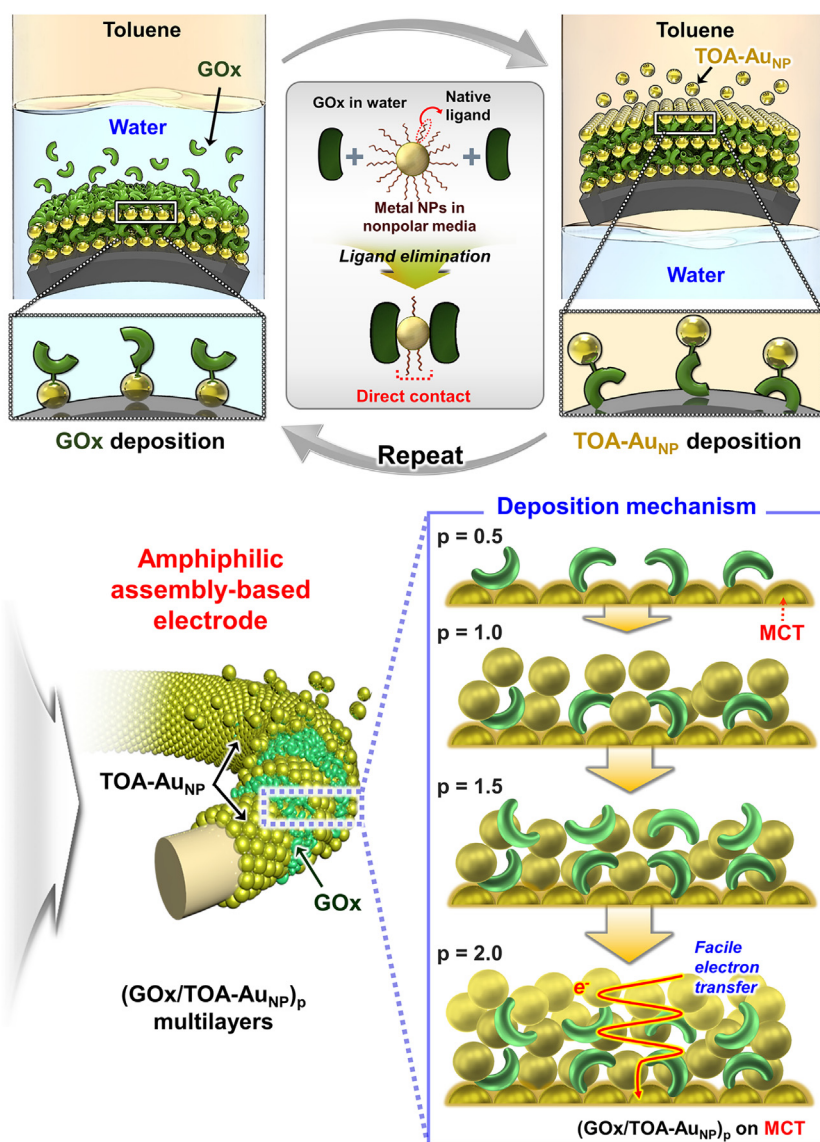
FIG. 1. Schematic illustrations of the new amphiphilic assembly. The amphiphilic assembly between hydrophilic enzymes in aqueous media and hydrophobic/conductive nanoparticles in nonpolar media for high-performance hybrid biofuel cells (BFCs). The amphiphilic assembly process based on the high affinity between the amino acid groups of enzymes (in aqueous solvent) and the surface of hydrophobic metal NPs (in a nonpolar solvent) forms the nanoblended GOx/hydrophobic NP film, which resultantly induces the direct contact between the enzyme and the metal NPs (the top panel). Additionally, the subsequent deposition of $(GOx/TOA-Au_{NP})_p$ multilayers on metallic cotton textiles (MCT) significantly enhances the electron transfer between adjacent GOx layers as well as between GOx layer and MCT (the bottom panel).

We quantitatively investigated the mass loading density of $(TOA-Au_{NP}/DETA)_n$ multilayers adsorbed onto a 3D porous cotton textile (thickness of $\sim 630 \, \mu m$) as a function of the bilayer number (n) (Figs. S6 and S7 in the supplementary material). In this case, the total mass density per bilayer was measured to be $\sim 0.58 \, mg \, cm^{-2}$, which was approximately 83 times higher than that on nonporous flat electrodes ($\sim 7.00 \times 10^{-3} \, mg \, cm^{-2}$ per bilayer). In addition, the electrical conductivity and sheet resistance of cotton textile electrodes exhibited strong correlations with the number of $TOA-Au_{NP}/DETA$ bilayers. As the bilayer number increased from 10 to 20, the electrical conductivity and sheet resistance of $(TOA-Au_{NP}/DETA)_n$-coated cotton changed from $0.02 \, S \, cm^{-1}$ and $43.25 \, \Omega \, sq^{-1}$ to $10.46 \, S \, cm^{-1}$ and $0.09 \, \Omega \, sq^{-1}$ (Fig. S8 in the supplementary material), respectively [these electrodes prepared from $(TOA-AuNP/DETA)_n$ multilayers are named as metallic cotton textiles (n-MCTs).

We also examined the electrochemical properties of n-MCTs as a function of the bilayer number at a scan rate of $5 \, mV \, s^{-1}$, employing a three-electrode cell configuration in $20 \, mmol \, l^{-1}$ phosphate-buffered saline (PBS) solution under ambient conditions. When the bilayer number was increased from 10 to 20, the cyclic voltammetry (CV) scans exhibited a gradual increase in the areal current density, implying that the LbL-assembled Au_{NPs} underwent electrooxidation and electroreduction reactions while maintaining their electrical conductivity (Fig. S9 in the supplementary material). It was reported that Pt_{NPs} and Au_{NPs} exhibit high oxygen reduction reaction (ORR) activity in BFC cathodes.[32–34] Therefore, our results strongly suggest the possibility that n-MCTs (particularly 20-MCTs) can be used as BFC cathodes as well as highly conductive host electrodes (a more detailed explanation is given in the caption of Fig. S9 in the supplementary material). Although increasing the bilayer number of $(TOA-Au_{NP}/DETA)_n$

multilayers can further improve the electrical conductivity of n-MCTs, the bilayer number for host electrodes was fixed at 20 for fabrication efficiency. The resulting 20-MCT exhibited a highly uniform surface morphology, large surface area, and high conductivity (an electrical conductivity of $\sim$10.46 S cm^{-1} and a sheet resistance of $\sim$0.09 Ω sq^{-1}) (Figs. S8 and S10 in the supplementary material).

B. Amphiphilic assembly of GOx-based anodes

Before the preparation of GOx-based anodes, we investigated the ability of hydrophobic TOA-Au$_{NPs}$ in toluene to be LbL-assembled with anionic GOx in water using UV-vis spectroscopy and QCM measurements (Figs. 1, S11–S13 in the supplementary material). As the periodic number (p) was increased from 1 to 10, the UV-vis absorbance of the (GOx/TOA-Au$_{NP}$)$_p$ multilayers linearly increased (Fig. S11 in the supplementary material), showing the typical absorbance peaks (at 277 nm) that represent GOx (Fig. S12 in the supplementary material) and Au$_{NPs}$ in solution [see Fig. S5(a)]. Additionally, the total loading amount of GOx and TOA-Au$_{NPs}$ per periodic layer was measured to be approximately 2.3 $\pm$ 0.3 μg cm^{-2} (Fig. S13 in the supplementary material). The total film thicknesses of the (GOx/TOA-Au$_{NP}$)$_p$ multilayers, as measured by field-emission scanning electron microscopy (FE-SEM), increased from approximately 18 to 193 nm as p was increased from 2 to 20 (Fig. S14 in the supplementary material). Additionally, in the case of the atomic force microscopy (AFM) measurements, the thicknesses of each adsorbed TOA-Au$_{NP}$ layer and each GOx layer were measured to be approximately 5.5 $\pm$ 1.3 and 3.3 $\pm$ 0.8 nm, respectively (Fig. S15 in the supplementary material). Given that the diameter of the TOA-Au$_{NPs}$ was approximately 6 nm, these results implied that the TOA-Au$_{NPs}$ were densely packed onto the substrate and that the hydrophilic (anionic) GOx was nanoblended with the hydrophobic conductive NPs through the amphiphilic ligand exchange reaction.[35] Furthermore, it should be here noted that the TOA-Au$_{NP}$ layers used for the preparation of the host electrode (MCT) were identically applied to the GOx multilayers, and additionally GOx were surrounded with Au$_{NPs}$. That is, this electrode structure and design suggest the possibility that the electron transfer within multilayers can be enhanced compared to that of other conventional GOx films without conductive components.

This unique amphiphilic assembly, performed in nonpolar and aqueous media with extremely different solvent polarities, occurred by consecutive ligand exchange reactions between the TOA ligands bound to the Au$_{NPs}$ and the amine (–NH$_2$) moieties within the amino acids of GOx. Although the characteristic absorption peaks of bare TOA-Au$_{NPs}$ in the FTIR spectra were partially overlapped with those of native GOx, the TOA ligands were replaced by the GOx containing amine groups during their LbL deposition as already mentioned (see Figs. S3 and S11 in the supplementary material). Therefore, in the case of LbL-assembled (GOx/TOA-Au$_{NP}$)$_3$ multilayers, their FTIR absorption bands almost coincided with those of native GOx. Particularly, considering that the FTIR absorption bands of active GOx exhibited the typical amide I (1650 cm^{-1}) and amide II (at 1539 cm^{-1}) absorption bands, our results evidently indicated that the immobilized GOx layers within multilayers were still in an active conformation (Fig. S16 in the supplementary material). Accordingly, the adsorption behavior between GOx and the TOA-Au$_{NPs}$ was investigated using amine-functionalized organic linkers and a carboxylic acid (COOH)-functionalized linker instead of GOx. More specifically, the

TOA-Au$_{NPs}$ in toluene were LbL-assembled with amine-functionalized PEI and DETA and carboxylic acid (COOH)-functionalized poly(acrylic acid) (PAA) in pH 7.4 water (Fig. S17 in the supplementary material). Considering that pK_a (the pH value at which 50% of the functional groups are ionized) of amine groups in aqueous solution is approximately 9,[36] the proportion of uncharged amine moieties within PEI and DETA was approximately 15%–25%. Although the TOA-Au$_{NPs}$ could be LbL-assembled with water-dissolved PEI or DETA, thereby showing a relatively high degree of ligand exchange [specifically, the degree of exchange (DOE) of TOA ligands in the pH 7.4 (DETA/TOA-Au$_{NP}$)$_{p=2}$ multilayers was estimated to be $\sim$68%], they had no affinity for the carboxylate ion (COO$^-$) groups of PAA [note that the pK_a of PAA is approximately 4.5, and therefore, most COOH groups of PAA are converted to carboxylate ion (COO$^-$) groups at pH 7.4]. These results suggest that the formation of GOx/TOA-Au$_{NP}$ multilayers was based on consecutive assembly through stable covalent bonding between the amine moieties of GOx and the surfaces of Au$_{NPs}$. Therefore, when hydrophilic (or anionic) GOx was the outermost layer, the water contact angle was measured to be approximately 48° $\pm$ 2°. However, upon the subsequent deposition of TOA-Au$_{NPs}$ onto the outermost GOx layer, the water contact angle increased up to 62° $\pm$ 1° (Fig. S18). These water contact angles periodically varied according to the identity of the outermost layer.

The effect of the outermost layer on the charge transfer of the enzyme electrode (i.e., the BFC anode) was investigated using electrochemical impedance spectroscopy (EIS). To this end, four different kinds of GOx-based multilayers [i.e., (GOx/TOA-Au$_{NP}$)$_p$, (GOx/DETA/citrate ion-stabilized Au$_{NP}$ (i.e., C-Au$_{NP}$)/DETA)$_p$, (GOx/DETA)$_p$, and (GOx/PEI)$_p$ multilayers] were LbL-assembled onto a nonporous flat electrode (Fig. S19 in the supplementary material). In addition, it should be noted that multilayered films using TOA-Au$_{NPs}$, cationic molecular linkers, and citrate Au$_{NPs}$ were newly designed to minimize the contact resistance between vertically adjacent GOx layers. The flat substrate used for these samples could minimize the effect of the macroporous structure of textile substrates on electrochemical performance. First, the equivalent series resistance (ESR) values of electrodes were measured under ambient conditions at a scan rate of 5 mV s^{-1} using a three-electrode cell configuration in PBS solution that contained 300 mmol l^{-1} glucose. When the first TOA-Au$_{NP}$ layer was adsorbed onto a single GOx layer-coated electrode, the ESR value of the formed (GOx/TOA-Au$_{NP}$)$_1$ electrode decreased from 62 (for the single-layer GOx electrode) to 55 Ω (for the outermost TOA-Au$_{NP}$-coated GOx electrode). However, when another GOx layer was adsorbed onto the (GOx/TOA-Au$_{NP}$)$_1$ electrode [i.e., making a (GOx/TOA-Au$_{NP}$)$_{1.5}$ electrode], the ESR value increased to 70 Ω. This alternating increase and decrease in ESR values were observed as the outermost layer was periodically changed [see the curves of the (GOx/TOA-Au$_{NP}$)$_p$ multilayers in Figs. S19(a) and S19(b) in the supplementary material]. This phenomenon indicates that compared to the electrostatic LbL-assembled films [specifically, the (GOx/DETA/C-Au$_{NP}$/DETA)$_p$, (GOx/DETA)$_p$, and (GOx/PEI)$_p$ multilayers], the (GOx/TOA-Au$_{NP}$)$_p$ multilayers could more effectively improve electron transfer through the periodic insertion of TOA-Au$_{NPs}$ between the vertically adjacent GOx layers and additionally prevent sharp increases in electrical resistance despite the higher loading mass of GOx (Experimental section, Figs. S19 and S20 in the supplementary material). A detailed explanation and the experimental methods for the

synthesis of C-Au$_{NPs}$ in water as well as the preparation of the electrostatic LbL-assembled (GOx/DETA/C-Au$_{NP}$/DETA)$_p$ and (GOx/DETA)$_p$ multilayers are given in the Experimental section and in Fig. S21 in the supplementary material.

While electrostatic LbL assembly (in aqueous/aqueous media) imposes a limit on increasing the packing density (or loading amount in lateral dimensions) of charged components (i.e., biomaterials and inorganic NPs) due to the strong electrostatic repulsion that occurs between same-charged species at pH 7.4 (Fig. S14 in the supplementary material), our amphiphilic assembly in aqueous/nonpolar media can resolve this critical drawback. Furthermore, the removal of unnecessary insulating organics during amphiphilic assembly and the uniform coating of an ultrathin GOx layer onto the densely packed conductive NP layer can minimize the obstacles that significantly interrupt electron transfer within a GOx-based anode. These unique characteristics of amphiphilic assembly starkly contrast with the adsorption behavior and electrode structure that results from traditional approaches.

## C. Electrochemical performance of amphiphilic assembly based anodes

Prior to studying the electrochemical behavior of the (GOx/TOA-Au$_{NP}$)$_p$ multilayers on MCTs (specifically 20-MCTs), we sought to examine the glucose oxidation ability of the bare MCT electrode. The anodic current density of a bare MCT electrode without GOx increased gradually as the glucose concentration was increased from 0 to 300 mmol l^{-1} in PBS (Fig. S22 in the supplementary material). Following this study, the electrochemical performance of the (GOx/TOA-Au$_{NP}$)$_p$ multilayer-coated MCTs was investigated by increasing p [Fig. 2(a)]. In this case, the anodic current density of (GOx/TOA-Au$_{NP}$)$_p$/MCT significantly increased up to p = 3 and then decreased [Fig. 2(b)]. A similar phenomenon was also observed for other anodes [i.e., (GOx/DETA/C-Au$_{NP}$/DETA)$_p$/MCT and (GOx/DETA)$_p$/MCT], which was mainly caused by the trade-off between the increased loading amount of GOx and the reduced electric field (due to the increase in the total film thickness). Therefore, in the case of (GOx/TOA-Au$_{NP}$)$_p$/MCT, the optimized p for a high-performance anode was determined to be 3, and its maximum anodic current density was measured to be ~8.9 mA cm^{-2} at a glucose concentration of 300 mmol l^{-1} [Fig. 2(b)]. We also confirmed that the electrochemical anodic performance of (GOx/TOA-Au$_{NP}$)$_3$/MCT was closely related to the concentration of glucose, implying that a higher glucose concentration resulted in a higher rate of electrooxidation via the enzymes adsorbed on the electrode (Fig. S23 in the supplementary material). Notably, the anodic current performance of (GOx/TOA-Au$_{NP}$)$_p$/MCT was greater than those of (GOx/DETA/C-Au$_{NP}$/DETA)$_p$/MCT and (GOx/DETA)$_p$/MCT.

Based on these results, we investigated the DET behaviors of GOx at the (GOx/TOA-Au$_{NP}$)$_p$/MCT electrode. Generally, in DET principle, the electrons are directly transferred from enzyme active site to electrode in the absence of additional mediators. It is also well-known that the conventional DET-based GOx electrodes prepared from the blending method exhibit a small oxidation peak of GOx near −0.45 V, which implies the typical DET behavior of GOx that (Fig. S24 in the supplementary material).[37–39] In line with these previous studies related to the DET behavior, the biocatalytic activity of LbL-assembled GOx to the oxidation of glucose was further investigated

using the CVs of the (GOx/TOA-Au$_{NP}$)$_p$/MCT electrode. As shown in Figs. S23(a) and S23(b) in the supplementary material, with increasing glucose concentration, the oxidation current level and redox peak intensity of GOx evidently increased during glucose oxidation. Such an increase in the oxidative current (at −0.41 V) indicated the direct contact between the electrode and the flavin adenine dinucleotide (FAD) center of GOx with two different specific oxidation (at −0.41 V vs Ag/AgCl at pH 7.4) and reduction peak potentials (−0.45 V vs Ag/AgCl at pH 7.4). That is, these peaks were attributed to the reduction and oxidation of electroactive center of the GOx by the DET process. On the other hand, a GOx-free electrode did not exhibit any redox peak in the potential range −0.6 to 0 V (Fig. S22 in the supplementary material). Additionally, in the case of denatured GOx-based anodes [i.e., a heat-treated and an ethanol-treated (GOx/TOA-Au$_{NP}$)$_p$/MCT electrode], we could not observe any corresponding electrochemical signals originating from denatured anodes. These phenomena evidently indicated that the catalytic oxidation process was caused by the catalytic reaction by active GOx, and resultantly the glucose oxidation at the anode is based on DET (Figs. S25 and S26 in the supplementary material). As further evidence, the CV scans of the (GOx/TOA-Au$_{NP}$)$_3$/MCT anode were also compared under ambient, nitrogen-saturated, and oxygen-saturated conditions at a scan rate of 5 mV s^{-1}. Although there was a noticeable difference in the CVs under oxygen conditions regarding glucose oxidation, no significant difference was observed under nitrogen and ambient conditions. Thus, the main cause of glucose oxidation is not oxygen but the direct electrochemical oxidation reaction of GOx due to its combination with metal NPs (Fig. S27 in the supplementary material).[40]

Based on the p associated with the maximum anodic current density, we also investigated the normalized anodic current densities of (GOx/TOA-Au$_{NP}$)$_3$/MCT, (GOx/DETA/C-Au$_{NP}$/DETA)$_4$/MCT, and (GOx/DETA)$_3$/MCT, along with the conventionally blended GOx/MCT [by the blending method using crosslinkable poly(ethylene glycol) diglycidyl ether (PEGDGE)] [Fig. 2(c)]. Particularly, it should be noted that three different kinds of LbL-assembled GOx multilayers except the blended GOx layer were newly designed to minimize the contact resistance between vertically adjacent GOx. First, the normalized anodic current density of (GOx/TOA-Au$_{NP}$)$_3$/MCT at +0.6 V was approximately 5.0 mA cm^{-2} at a glucose concentration of 300 mmol l^{-1}. In this case, the background current density (i.e., 3.9 mA cm^{-2} at +0.6 V) of (GOx/TOA-Au$_{NP}$)$_3$/MCT at 0 mmol l^{-1} glucose was subtracted from the measured current density of the (GOx/TOA-Au$_{NP}$)$_3$/MCT electrode at 300 mmol l^{-1} glucose to obtain the normalized anodic current density. As a result, the (GOx/TOA-Au$_{NP}$)$_3$/MCT anode exhibited a much higher normalized anodic current density (~5.0 mA cm^{-2} at +0.6 V) than the (GOx/DETA/C-Au$_{NP}$/DETA)$_4$/MCT (~2.3 mA cm^{-2}), (GOx/DETA)$_3$/MCT (~1.5 mA cm^{-2}), and conventionally blended GOx/MCT (~0.6 mA cm^{-2}) electrodes [Figs. 2(c) and S28−S30 in the supplementary material]. Despite the relatively poor anodic performance of (GOx/DETA)$_3$/MCT in our study, it should be noted that the performance of (GOx/DETA)$_3$/MCT was higher than that of the conventionally blended GOx-based textile anodes reported thus far.

We also envisioned the possibility that another enzyme could be directly combined with hydrophobic metal NPs without additional surface modification. To demonstrate the utility of the electrode architecture, catalase (CAT) in water was LbL-assembled with hydrophobic
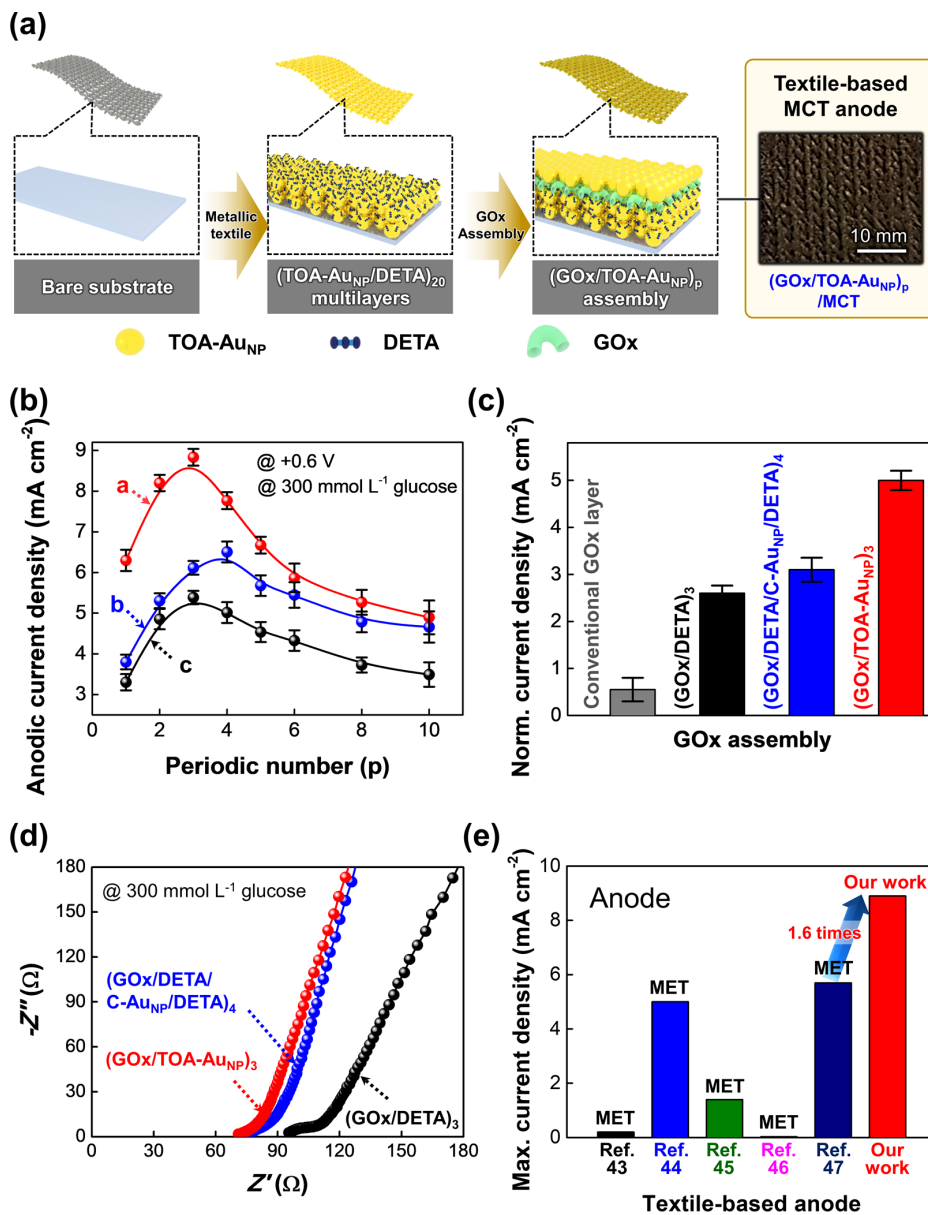
FIG. 2. Amphiphilic assembly-based anodes composed of $(GOx/TOA\text{-}Au_{NP})_p$ multilayers and their anodic performance. (a) Schematic (left) and optical micrograph (right) of the $(GOx/TOA\text{-}Au_{NP})_p$-assembled MCT anode. (b) Dependence of the current density on the periodic number (p) for three different anodes [(a) $(GOx/TOA\text{-}Au_{NP})_3$/MCT (red), (b) $(GOx/DETA/C\text{-}Au_{NP}/DETA)_4$/MCT (blue), and (c) $(GOx/DETA)_3$/MCT (black)]. (c) Comparison of the normalized current densities for three different LbL-assembled GOx-containing electrodes and the GOx electrode formed with the conventional blending method tested at a glucose concentration of 300 mmol l^{-1}. (d) Nyquist plots of three LbL-assembled GOx-containing anodes in PBS with 300 mmol l^{-1} glucose solution. (e) Comparison of the maximum anodic current density of $(GOx/TOA\text{-}Au_{NP})_3$/MCT in this work with those of previously reported textile-based anodes.[43–47]

$TOA\text{-}Au_{NPs}$ in toluene, which was confirmed by UV-vis spectroscopy (Fig. S31 in the supplementary material). Additionally, the electrocatalytic activity of $CAT/TOA\text{-}Au_{NP}$ multilayers was significantly increased with increasing the concentration of H_2O_2 [Fig. S31(b) in the supplementary material]. These results highlight the versatility of active components in amphiphilic assemblies and the universal benefits of this novel approach in improving the electrochemical performance. Accordingly, we confirmed that our amphiphilic assembly could also be effectively applied to electrochemical sensors using CAT as well as BFCs using enzymes.

The enhanced electrochemical performance of $(GOx/TOA\text{-}Au_{NP})_3$/MCT was also based on the stability of GOx in both water and toluene. That is, the hydration layer surrounding GOx in nonpolar media such as toluene could preserve enzyme activity without substantial loss when the electrode was returned to the aqueous solution while also protecting GOx from enzyme denaturation during assembly with hydrophobic NPs in nonpolar media.[41] To test these possibilities, the activity of the assembled GOx layers was investigated as a function of dipping time when the GOx-coated electrodes were dipped in toluene and water (Fig. S32 in the supplementary material). In this case, DETA was used instead of the $TOA\text{-}Au_{NPs}$ to prevent GOx from being exposed to toluene during multilayer formation. Specifically, anionic GOx underwent electrostatic LbL-assembly with cationic DETA in pH 7.4 water for the preparation of $(GOx/DETA)_3$

multilayers on Au-coated Si wafers. After immersing the formed multilayer-coated electrodes in toluene or water for the given dipping time, the activity of the GOx electrodes was investigated at 300 mmol l^{-1} glucose. The activity of the GOx electrodes immersed in toluene was similar to that in water. However, when acetone or ethanol was used instead of toluene, GOx demonstrated decreased activity because the hydrophilic organic solvent easily penetrated its hydration layer.[39] Furthermore, in the case of the (GOx/TOA-Au$_{NP}$)$_3$/MCT electrode, residual toluene was not detected (Fig. S33 in the supplementary material).

To obtain detailed information about the electron transfer characteristics of anodes, ESR values of (GOx/TOA-Au$_{NP}$)$_3$/MCT, (GOx/DETA/C-Au$_{NP}$/DETA)$_4$/MCT, and (GOx/DETA)$_3$/MCT were evaluated at a glucose concentration of 300 mmol l^{-1} using EIS. As shown in Fig. 2(d), the 27 nm-thick (GOx/TOA-Au$_{NP}$)$_3$ multilayers on MCTs exhibited a lower ESR value ($\sim$72 Ω at 1 kHz) than the 23 nm-thick (GOx/DETA/C-Au$_{NP}$/DETA)$_4$ multilayers with a low NP packing density ($\sim$74 Ω at 1 kHz) and the 12 nm-thick (GOx/DETA)$_3$ multilayers with insufficient surface coverage ($\sim$97 Ω at 1 kHz) (Fig. S14 in the supplementary material). Considering that the ESR value is determined by the sum of the resistances generated by each component (i.e., the electrolyte, active GOx, and host electrode) and the interfaces (mainly GOx and the host electrode), these results imply that the electron transfer of (GOx/TOA-Au$_{NP}$)$_3$/MCT with its lower internal resistance is more facile and effective than that of other anodes. Particularly, as mentioned earlier, given that the TOA-Au$_{NP}$ inserted between adjacent GOx layers were exactly identical to those used for the preparation of MCT [i.e., (TOA-Au$_{NP}$/DETA)$_{20}$-coated cotton textile], it is reasonable to conclude that the inserted TOA-Au$_{NP}$ layers could enhance the DET between GOx multilayers and MCT electrode (Fig. 1).

The surface coverage (Γ) of the LbL-assembled GOx on MCTs in (GOx/TOA-Au$_{NP}$)$_3$/MCT, (GOx/DETA/C-Au$_{NP}$/DETA)$_4$/MCT, and (GOx/DETA)$_3$/MCT was calculated to be approximately 4.7×10^{-7}, 3.4×10^{-7}, and 2.1×10^{-7} mol cm^{-2}, respectively (Experimental section for the calculation method). These results clearly demonstrate that (GOx/TOA-Au$_{NP}$)$_3$/MCT had a larger amount of immobilized GOx than the electrostatic LbL assemblies. In addition, the electron transfer kinetics of the (GOx/TOA-Au$_{NP}$)$_3$/MCT anode were further investigated using the Laviron model for a quasi-reversible and surface-controlled electrochemical system.[42] The apparent heterogeneous electron transfer rate constant (K_s) was estimated to be 5.3 ± 0.2 s^{-1}, which was much higher than those (0.3–3.96 s^{-1}) of previously reported BFC anodes (Fig. S34 in the supplementary material). These results suggest that the electron transfer between GOx and the MCT electrode was considerably enhanced due to the strong electron relay effect of densely packed TOA-Au$_{NP}$s sandwiched between neighboring GOx layers. As a result, the anodic current density of our anode [i.e., the (GOx/TOA-Au$_{NP}$)$_3$/MCT anode] was greater than those of all anodes (including textile-based MET anodes) reported thus far [Fig. 2(e)].[43–47]

D. Electrochemical performance of cathode

An MCT composed of Au$_{NP}$ multilayers can be used as the BFC cathode as well as the host electrode due to the ORR electrocatalytic activity of Au$_{NP}$s.[17,22,32] However, in our study, to further enhance the ORR activity of the MCTs, Pt, which has excellent ORR activity, was

sputtered onto the outermost DETA layer of MCTs for a short time ($<$2 min) via a vacuum deposition process (for the preparation of Pt-MCT) (Fig. S35 in the supplementary material). The sputtered Pt was deeply incorporated into the entire region, ranging from the top surface to the bottom of the 630 μm-thick MCTs. This phenomenon was clearly confirmed by the cross-sectional FE-SEM and energy dispersive x-ray spectroscopy (EDS) mapping images (Fig. S36 in the supplementary material). Additionally, the sputtered Pt had a high affinity (i.e., covalent bonding) for the NH$_2$-functionalized MCT (i.e., the outermost DETA layer-coated MCT), resulting in the formation of a robust cathode. Based on these results, Pt was sputtered onto both sides of the MCT for the preparation of the BFC cathode (Pt-MCT). The current density of a Pt-MCT cathode at a potential of -0.6 V notably increased from -4.2 to -16.7 mA cm^{-2} when increasing the sputtering time from 0 to 90 s (Fig. S37 in the supplementary material). The ORR activity of the Pt-MCT electrode was measured under three different conditions (nitrogen-saturated, ambient, and oxygen-saturated PBS solutions) using CV scans. The cathodic current densities of the MCTs (at a potential of -0.6 V) under ambient and oxygen-saturated conditions were approximately -16.7 and -37.5 mA cm^{-2}, respectively (Fig. S38 in the supplementary material). On the other hand, the current density of the one-sided Pt-MCTs increased from -4.2 to -7.3 mA cm^{-2} over the above-mentioned increase in sputtering time (Fig. S39 in the supplementary material).

E. Textile- or fiber-type BFCs based on amphiphilic assembly

Based on the optimal structure and design of enzyme fibril BFC electrodes, we prepared complete 3D porous textile-based DET-BFCs [Figs. 3(a) and S40 in the supplementary material]. To exclude parasitic currents at the anode and cathode, stationary power outputs were measured by the external circuit resistance method. First, the power density of BFCs with the Pt-sputtered cathode was approximately 30% greater than that of BFCs with the Pt-free cathode (Fig. S41 in the supplementary material). Specifically, when the power density of a BFC [i.e., (GOx/TOA-Au$_{NP}$)$_3$/MCT//Pt-MCT] was measured using the external circuit resistance method, the resulting power output in 300 mmol l^{-1} glucose under ambient conditions was $\sim$1.5 mW cm^{-2} with an open-circuit voltage (OCV) of $\sim$0.80 [Figs. 3(b) and S42(a) in the supplementary material]. On the other hand, the maximum power densities of (GOx/DETA/C-Au$_{NP}$/DETA)$_4$/MCT//Pt-MCT and (GOx/DETA)$_3$/MCT//Pt-MCT were approximately 1.3 and 1.1 mW cm^{-2}, respectively. Although the DET-BFC composed of the (GOx/DETA)$_3$/MCT anode and Pt-MCT cathode exhibited a relatively low power density of 1.1 mW cm^{-2}, this power density exceeded the maximum power densities ($<$0.25 mW cm^{-2}) of previously reported textile-type MET-BFCs.[44–46] When using a low glucose concentration of 10 mmol l^{-1} (corresponding to physiological conditions), (GOx/TOA-Au$_{NP}$)$_3$/MCT//Pt-MCT exhibited a power density of approximately 0.73 mW cm^{-2} with an OCV of $\sim$0.8 V [Figs. 3(c) and S42(b) in the supplementary material]. The (GOx/DETA/C-Au$_{NP}$/DETA)$_4$/MCT- and (GOx/DETA)$_3$/MCT-based BFCs exhibited power densities of 0.67 mW cm^{-2} (with an OCV of 0.7 V) and 0.60 mW cm^{-2} (with an OCV of 0.6 V), respectively.

Importantly, the amphiphilic assembly based BFC displayed good stability. Specifically, this BFC maintained approximately 81% ($\sim$0.60 mW cm^{-2}) of its initial power density even after continuous
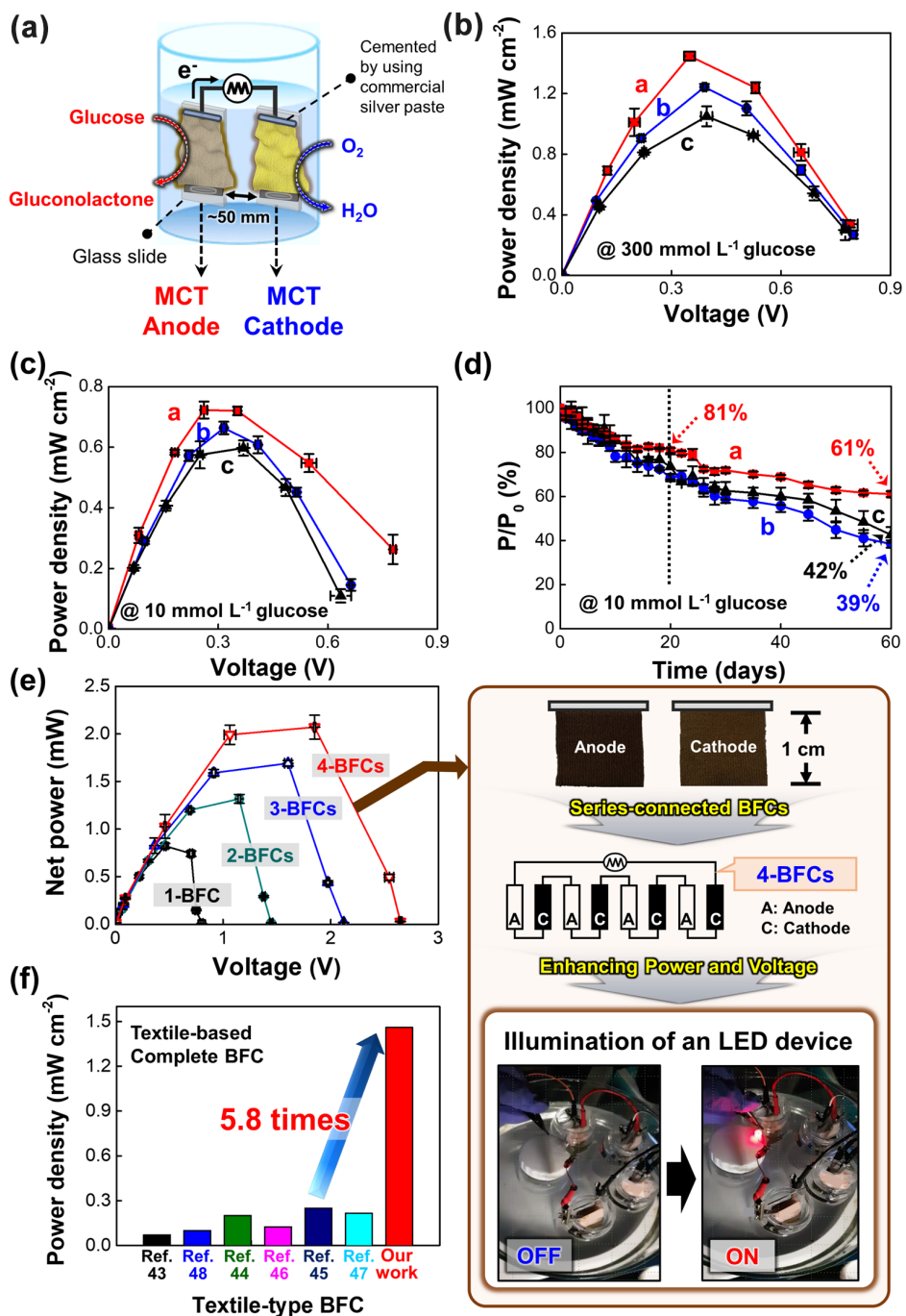
FIG. 3. Performance of complete 3D porous metallic cotton textile (MCT)-BFCs. (a) Schematic diagram showing a complete BFC operated in the glucose-containing buffer. Anode reaction: glucose $\rightarrow$ gluconolactone $+ 2H^+ + 2e^-$, cathode reaction: $O_2 + 4H^+ + 4e^- \rightarrow 2H_2O$, and complete BFC system reaction: $2glucose + O_2 \rightarrow 2gluconolactone + 2H_2O$. (b) Power outputs of MCT-BFCs with three different anodes [(a) (GOx/TOA-Au$_{NP}$)$_3$/MCT, (b) (GOx/DETA/C-Au$_{NP}$/DETA)$_4$/MCT, and (c) (GOx/DETA)$_3$/MCT] and Pt-MCT cathodes (with a 90 s sputtering time) tested in PBS with 300 mmol l^{-1} glucose at 36.5 °C. In this case, the geometric surface area of the BFC electrode was fixed at 0.25 cm^2. (c) Power outputs of MCT-BFCs with three different anodes in 10 mmol l^{-1} glucose in PBS at 36.5 °C. (d) Relative power retention (P/P$_0$) of the complete BFCs with three different anodes in 10 mmol l^{-1} glucose in PBS over 60 days. The power output of each complete BFC was continuously measured with external resistors as a function of time. (e) Net power outputs of four BFC systems (surface area of $\sim$1 cm^2 for a single BFC) in 300 mmol l^{-1} glucose buffer and their BFC connections. Photographs showing the series-connected BFC operation and illumination of an LED (OFF: not connected, ON: connected). (f) Comparison of the single textile-based BFC power values reported to date.[43–48]

operation in PBS solution containing 10 mmol l^{-1} glucose for 20 days (approximately 61% of the initial power density after 60 days) [Figs. 3(d) and S43 in the supplementary material]. However, the electrostatic assembly based BFCs exhibited much lower stability than amphiphilic assembly based BFCs. These results show that the formation of stable covalent bonds between the amine groups of GOx and the surface of the Au$_{NPs}$ as well as between the host electrode and GOx significantly contributed to the robust immobilization of GOx.

In addition to the power density, the net power of BFCs is very important for practical biomedical applications. Therefore, we aimed to enhance the net power performance of the amphiphilic assembly-based BFCs [i.e., (GOx/TOA-Au$_{NP}$)$_3$/MCT//Pt-MCTs]. To achieve this goal, the geometric surface areas of the textile electrodes were first increased from 0.25 to 1 cm^2, which increased the net power of the BFCs from ∼0.3 to ∼0.8 mW with an OCV of ∼0.8 V. When four BFCs were connected in series, the maximum power output was further increased to ∼2.1 mW with a voltage of ∼2.7 V [Figs. 3(e) and S44 in the supplementary material]. The four series-connected BFC (4-BFC) system directly illuminated a red LED requiring a voltage of over 1.7 V without any additional accessories (i.e., a DC/DC converter and/or a capacitor), unlike previously reported MET-BFCs. We highlight that the high areal power density (∼1.5 mW cm^{-2}) and high net power (∼2.1 mW) shown in our study have not been reported to date [Fig. 3(f) and Table S1 in the supplementary material].[43–48] Specifically, the areal power performance of (GOx/TOA-Au$_{NP}$)$_3$/MCT//Pt-MCT was 5.8 times higher than the best reported value (0.25 mW cm^{-2} for a nylon-spandex textile-based electrode) of textile-based MET-BFCs, and the net power performance was 5.5 times higher than the best reported value (0.38 mW for a cotton textile cloth-based electrode) of textile-based MET-BFCs.[46] Our assembly approach is also advantageous for increasing the size of BFC electrodes (Fig. S45 in the supplementary material).

Furthermore, we investigated the current performance of the fiber-based electrodes (i.e., the anode and cathode) and the areal power performance of a complete BFC [Fig. 4(a)]. In this case, the (TOA-Au$_{NP}$/DETA)$_n$-coated cotton fiber, which could have a lower overall internal resistance than the above-mentioned textile electrode, was used as a host electrode. The additional deposition of (GOx/TOA-Au$_{NP}$)$_3$ multilayers and Pt sputtering onto metallic cotton fiber (MCF) produced an anode [i.e., (GOx/TOA-Au$_{NP}$)$_3$/MCF anode] and a cathode (i.e., Pt-n–MCF cathode) for fiber-type BFCs, respectively. To further improve both the electrical conductivity and electron transfer efficiency of the BFC electrode, additional TOA-Au$_{NP}$ layers were inserted within both the anode and cathode. In this case, the GOx layers sandwiched between more densely packed TOA-Au$_{NP}$ layers can enhance the DET between neighboring GOx within multilayers as well as between MCT and GOx multilayers. As shown in Figs. 4(b) and S48 in the supplementary material, the anodic [Figs. 4(b) and S46(a) and S46(b) in the supplementary material] and cathodic current densities [Figs. 4(c) and S46(c) and S46(d) in the supplementary material] increased to 93 and −197 mA cm^{-2}, respectively. Based on these improvements, the prepared (GOx/TOA-Au$_{NP}$/DETA/TOA-Au$_{NP}$)$_3$/MCF//Pt-100-MCF BFC exhibited a maximum areal power density of ∼7.3 mW cm^{-2} in 300 mmol l^{-1} glucose under ambient conditions with a fixed external resistance. This result outperformed previously reported fiber-type BFCs, including MET-BFCs [Figs. 4(d), S47, and Table S2 in the supplementary material]. Furthermore, the

amphiphilic assembly-based BFC with additional TOA-Au$_{NP}$ layers exhibited improved operational stability: ∼86% and ∼70% of the initial power output (∼1.2 and ∼3.8 mW cm^{-2}) were maintained in 10 and 100 mmol l^{-1} glucose, respectively, after 12 days of continuous operation (Fig. S48 in the supplementary material).

III. CONCLUSIONS

In this study, we demonstrated that amphiphilic assembly could be effectively applied to design hybrid BFC anodes; additionally, the resultant 3D porous textile- or fiber-based DET-BFCs exhibited remarkable areal power densities and net power outputs. In particular, we showed that the amphiphilic assembly between water-soluble enzymes and hydrophobic/conductive NPs significantly improved the electron transfer efficiency between the enzyme and electrode as well as between neighboring enzymes, resulting in highly uniform layers and a robust electrode structure. The resulting hybrid BFC based on amphiphilic assembly generated an exceptionally high areal power density and a high net power output under a fixed external resistance. Considering the versatility of using conductive and electrocatalytic components in amphiphilic assembly, the introduced approach can provide a basis for designing a variety of high-performance electrodes with enhanced electrical conductivity and electrocatalytic performance.

IV. EXPERIMENTAL METHODS

A. Materials

Cotton textile (thickness of 630 μm) was purchased from KohasiD Co., Ltd. (Republic of Korea), and glucose oxidase (GOx) derived from *Aspergillus niger* (180 U mg^{-1}) was purchased from Amano Enzyme, Inc. (Japan). All chemical reagents were purchased from Sigma-Aldrich and used without further purification.

B. Synthesis of TOA-Au$_{NPs}$

Tetraoctylammonium bromide (TOA)-stabilized Au NPs (i.e., TOA-Au$_{NPs}$) with average diameters of 6 nm were synthesized using a two-phase method in toluene.[30] Briefly, HAuCl$_4$·3H$_2$O in water (30 mmol l^{-1}, 30 ml) and TOA stabilizers in toluene (20 mmol l^{-1}, 80 ml) were mixed with vigorous stirring, and then NaBH$_4$ (a reducing agent for synthesizing TOA-Au$_{NPs}$) in water (0.4 mol l^{-1}, 25 ml) was added to the two-phase mixture. When HAuCl$_4$·3H$_2$O-dissolved water was mixed with TOABr-dissolved toluene, AuCl$_4^-$ ions in the water phase are rapidly transferred to the toluene phase containing tetraoctylammonium (TOA$^+$) ions, resulting in the formation of TOA$^+$AuCl$_4^-$ in the toluene phase.[30,49,50] In this case, the addition of NaBH$_4$-dissolved aqueous solution to the toluene phase containing TOA$^+$AuCl$_4^-$ induces the formation of TOA-Au$_{NPs}$ as a result of chemical reduction. After stirring for approximately 3 h, the aqueous solution was separated from the mixture, and then the remaining toluene solution was repeatedly washed using dilute aqueous H$_2$SO$_4$ (0.1 mol l^{-1}), NaOH (0.1 mol l^{-1}), and de-ionized water. After several washing steps and the removal of the aqueous solution, TOA-Au$_{NPs}$ dispersed in toluene were obtained.

C. Synthesis of C-Au$_{NPs}$

Anionic citrate ion-stabilized Au$_{NPs}$ (C-Au$_{NPs}$) with average diameters of ∼23 nm were synthesized.[42] Briefly, a 100 ml sample of aqueous HAuCl$_4$ (0.1 mmol l^{-1}) was put into a 250 ml flask at room
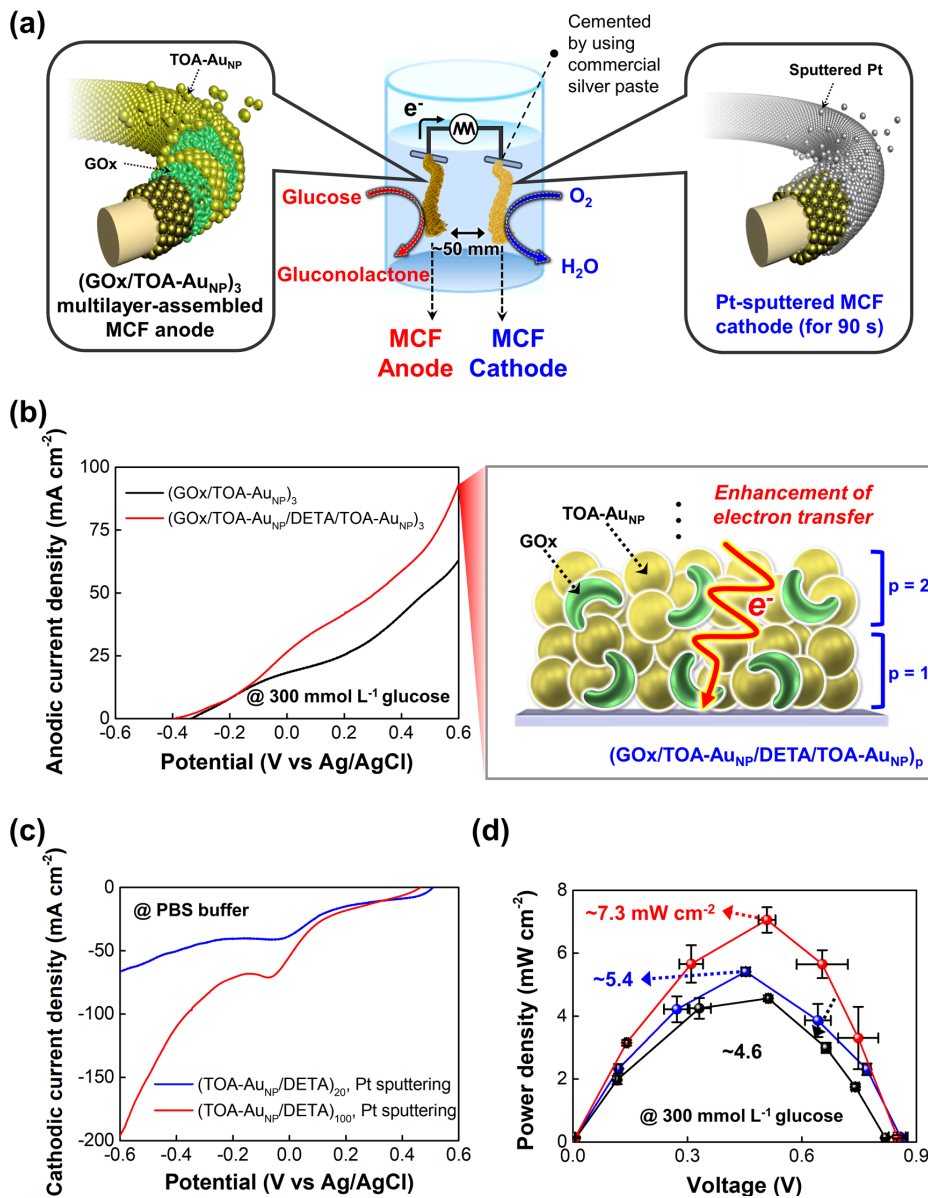
FIG. 4. Performance of metallic cotton fiber (MCF)-based anodes, cathodes, and complete BFCs. (a) Schematic showing a complete MCF-BFC operated in glucose-containing buffer. (b) Anodic current density curves of the $(GOx/TOA-Au_{NP})_3/MCF$ and $(GOx/TOA-Au_{NP}/DETA/TOA-Au_{NP})_3/MCF$. In this case, the symbol of DETA was omitted in the scheme because DETA as an extremely small molecule does not have a meaningful effect on the charge transfer of the electrode. (c) Cathodic current density curves of Pt-20-MCF and Pt-100-MCF cathodes. (d) Power (P)–voltage (V) profiles of single MCF-BFCs with the $(GOx/TOA-Au_{NP})_3/MCF//Pt-20-MCF$ (black), $(GOx/TOA-Au_{NP})_3/MCF//Pt-100-MCF$ (blue), and $(GOx/TOA-Au_{NP}/DETA/TOA-Au_{NP})_3/MCF//Pt-100-MCF$ (red). The power output was obtained in PBS solution containing 300 mmol l^{-1} glucose (under ambient conditions at 36.5 °C) by measuring the current flowing through external variable resistors (from 1 kΩ to 10 GΩ) to control the cell potential.

temperature. The solution was heated under magnetic stirring ($\sim$750 rpm), and after it started to boil, 1.2 ml of sodium citrate solution (50 mg ml^{-1}) was added. The reaction was allowed to proceed until the solution became wine red in color (after approximately five minutes). After no further color change was observed, the solution was cooled slowly to room temperature.

D. Fabrication of MCT electrodes

Cotton textiles were dipped in ethanolic solutions of poly(ethylene imine) (PEI, $M_w \approx 800$ g mol^{-1}, 1 mg ml^{-1}) for 40 min. The resulting PEI-coated textiles, which were prepared via hydrogen-

bonding interactions between the NH$_2$ groups of PEI and the OH groups of the cotton surface, were immersed in a TOA-Au$_{NP}$ suspension (10 mg ml^{-1}) for 40 min and then washed in toluene to remove the weakly adsorbed TOA-Au$_{NPs}$. The bulky TOA ligands bound to the surface of the Au$_{NPs}$ were replaced by the NH$_2$ groups of the PEI-coated cotton textiles due to the high affinity between the Au surface and the NH$_2$ groups. Next, the formed TOA-Au$_{NP}$-coated cotton textiles were immersed in a solution of diethylenetriamine (DETA) in ethanol (1 mg ml^{-1}) for 40 min. This process was repeated, and the cotton textiles were washed in ethanol to remove the excess DETA molecules, resulting in cotton textiles coated with one bilayer [i.e., (TOA-Au$_{NP}$/DETA)$_1$-cotton textile]. The adsorption mechanism

between TOA-Au$_{NPs}$ and NH$_2$-functionalized DETA is the same as that between TOA-Au$_{NPs}$ and PEI. These deposition and washing steps for the preparation of the MCTs were continuously repeated. (TOA-Au$_{NP}$/DETA)$_{20}$-cotton textiles were used as the host anodes and cathodes of BFCs.

E. Fabrication of (GOx/TOA-Au$_{NP}$)$_p$/MCT anodes

A fabricated MCT electrode was immersed in a solution of GOx (5 mg ml^{-1} in PBS containing 0.5 M NaCl) for 20 min and then washed with distilled water (pH 5.8) to remove weakly adsorbed GOx. Then, TOA-Au$_{NPs}$ dispersed in toluene were deposited for 20 min on top of the GOx layer and washed with toluene to remove the weakly adsorbed TOA-Au$_{NPs}$. During the deposition and washing steps, hydrophilic GOx molecules in aqueous solution were stably adsorbed onto the hydrophobic TOA-Au$_{NPs}$ in the MCT. This process was repeated to obtain the desired number (p) of multilayers.

F. Fabrication of (GOx/DETA/C-Au$_{NP}$/DETA)$_p$/MCT anodes

The fabricated MCT electrode was immersed first in a solution of GOx (5 mg ml^{-1} in PBS containing 0.5 M of NaCl), then in DETA (1 mg ml^{-1} in 0.5 M NaCl) and finally in the prepared C-Au$_{NP}$ suspension for 20 min each and washed with distilled water (pH 5.8) between steps. This electrostatic deposition was induced by two negatively charged materials (GOx molecules in PBS solution and C-Au$_{NPs}$ in water) and positively charged DETA. These steps were repeated until the anode with the desired p [i.e., (GOx/DETA/C-Au$_{NP}$/DETA)$_p$/MCT] was obtained.

G. Fabrication of (GOx/DETA)$_p$/MCT anodes

The fabricated MCT electrode was immersed in a solution of GOx (5 mg ml^{-1} in water containing 0.5 M NaCl) for 20 min and then washed with distilled water (pH 5.8). This was followed by immersion in a solution of DETA (1 mg ml^{-1} in water containing 0.5 M NaCl) for 20 min and another washing with distilled water. During the deposition and washing steps, negatively charged GOx molecules were electrostatically adsorbed onto the positively charged DETA on the MCTs. These steps were repeated until an anode with the desired p [(GOx/DETA)$_p$/MCT] was obtained.

H. Fabrication of GOx/MCT anodes

The GOx/MCT anode was prepared by blending GOx with a cross-linking polymer [i.e., poly(ethylene glycol) diglycidyl ether (PEGDGE 400) (7 wt. %)]. Then, the MCT was immersed in the formed slurry for one day and dried under ambient conditions.[8]

I. Fabrication of Pt-MCT cathodes

For BFC cathodes, Pt was additionally deposited on the MCTs through a vacuum sputtering process using an ion sputter coater (MC1000, Hitachi) with argon (Ar) gas flow at a vacuum pressure of $\approx 10^{-2}$ Torr at a discharge current of 15 mA. The deposition time was varied up to 90 s.

J. Characterizations and analyses of multilayer formation and MCT-based BFC electrodes

The surface and cross-sectional morphologies of the MCT-based BFC electrodes were characterized using FE-SEM (Hitachi S4700, Japan) and AFM (XE-100, Park Systems, South Korea). X-ray photoelectron spectroscopy (XPS) was conducted using an X-TOOL (ULVAC-PHI, Japan) equipped with an Al Kα x-ray source (1486.6 eV, 24.1 W, 15 kV). The main chamber was maintained at a pressure less than 4.25×10^{-7} Pa. Binding energies were referenced to the Au 4f$_{7/2}$ signal at 84.0 eV. All spectra were acquired with an analyzer pass energy of 140 eV. The loading mass of the (TOA-Au$_{NP}$/DETA)$_n$ multilayers adsorbed onto the cotton textile electrode was measured using an analytical balance (XP205 model, Mettler Toledo, resolution of 0.01 mg). The adsorption behavior and mechanism of formation of the multilayers were investigated using an FTIR spectrometer in specular mode (Cary 600 spectrometer, Agilent Technologies, USA). The growth and loading amount of the LbL-assembled multilayers were examined using UV-vis spectroscopy (Lambda 35, Perkin Elmer) on quartz glass and a QCM (QCM 200, SRS, USA), respectively. In the case of the QCM measurement, the mass change (Δm) per layer was calculated from the QCM frequency change (ΔF) using the Sauerbrey equation,[51]

$$\Delta F(Hz) = -\frac{2F_0^2}{A\sqrt{\rho_q \mu_q}} \cdot \Delta m,$$

where F_0, A, ρ_q, and μ_q represent the resonant frequency ($\sim$5 MHz), the active area (cm^2), the density (2.65 g cm^{-3}), and the shear modulus (2.95×10^{11} g cm^{-1} s^{-2}) of the QCM electrode, respectively. This expression can be simplified to ΔF (Hz) $= -56.6 \times \Delta m_A$ (the change in mass per unit area, or $\Delta m/A$).

K. Calculation of surface coverage of GOx

The surface coverage (Γ) of the LbL-assembled GOx on MCTs was calculated using the charge integration of the anodic peak in the CV scans,

$$\Gamma = Q/nFA,$$

where Q is the total amount of charge, A is the working electrode area, F is the Faraday constant, and n is the number of electrons transferred (n = 2).[52]

L. Electrochemical measurements

In a three-electrode system composed of an MCT working electrode, a Ag/AgCl reference electrode, and a Pt counter electrode, the top end of the working electrode was firmly connected to a copper wire using commercial silver paste (ELCOAT P-100, CANS, South Korea) on a glass substrate to avoid electrical shortages during continuous operation. After the silver paste was dry, it was additionally insulated with epoxy adhesive to avoid shortages. CVs of an MCT electrode (active geometric surface area of 0.25 cm^2 for single BFC systems and 1 cm^2 for series-connected BFC systems) were measured over the potential range -0.6 to $+0.6$ V using an electrochemical analyzer (Ivium-n-Stat, Ivium Technologies, the Netherlands). All measurements were carried out in an electrochemical cell in 50 ml of PBS solution (20 mmol l^{-1} phosphate and 0.14 mol l^{-1} NaCl, pH 7.4) at

36.5 °C without stirring. The interelectrode spacing between the anode and cathode electrodes was ~50 mm, and in this study, no membrane was used between the two electrodes. The anodic and cathodic current densities were determined by CV; the maximum current density was observed at a voltage of +0.6 V for the anode and −0.6 V for the cathode. The normalized current density was obtained by subtracting the current density in glucose-free PBS at +0.6 V for the anode and by subtracting the current density in oxygen-free PBS at −0.6 V for the cathode.

The BFC power densities were determined by measuring the current flowing through external variable resistors (from 1 kΩ to 10 GΩ) to control the cell potential. EIS measurements for the BFC electrodes were performed over the frequency range of 0.2 Hz to 100 kHz with a perturbation amplitude of 0.01 V. The impedance spectra (Nyquist plots) of the real (Z') and imaginary parts (Z'') obtained from the electrochemical BFC cells were processed using ZView software (version 2.8d, Scribner Associates Inc., USA).

SUPPLEMENTARY MATERIAL

See the supplementary material for details on the UV-vis spectra and TEM image of materials, FTIR spectra and QCM data of assembled film, additional SEM data, XPS data, electrochemical performances of the textile- and fiber-BFC electrodes (GOx/TOA-Au$_{NP}$)$_3$/MCT anode and Pt-MCT cathode), characterization of the amphiphilic assembly based BFCs system, and the operational stability tests.

ACKNOWLEDGMENTS

AUTHOR DECLARATIONS
Conflict of Interest

The authors have no conflicts to disclose.

Author Contributions

C.H.K. and J.C. conceived the idea and designed the experiments. C.H.K., M.K., M.K., D.N., Y.S., and E.Y. performed all the experiments. M.O., Y.K., B.Y., and J.H.M. discussed the experimental results. C.H.K., S.W.L., and J.C. wrote the manuscript. All authors discussed the results and commented on the manuscript.

DATA AVAILABILITY

The data that support the findings of this study are available within the article and its supplementary material.

REFERENCES

[1] S. J. Updike and G. P. Hicks, Nature **214**, 986 (1967).
[2] X. Xiao, H. Xia, R. Wu, L. Bai, L. Yan, E. Manager, S. Cosnier, E. Lojou, Z. Zhu, and A. Liu, Chem. Rev. **119**(16), 9509 (2019).
[3] K. Elouarzaki, D. Cheng, A. C. Fisher, and J.-M. Lee, Nat. Energy **3**, 574 (2018).
[4] R. Ghosh, K. Y. Pin, V. S. Reddy, W. A. D. M. Jayathilaka, D. Ji, W. Serrano-García, S. K. Bhargava, S. Ramakrishna, and A. Chinnappan, Appl. Phys. Rev. **7**, 041309 (2020).
[5] M. J. Moehlenbrock and S. D. Minteer, Chem. Soc. Rev. **37**(6), 1188 (2008).
[6] N. Mano, F. Mao, and A. Heller, J. Am. Chem. Soc. **124**(44), 12962 (2002).
[7] P. Kavanagh and D. Leech, Phys. Chem. Chem. Phys. **15**(14), 4859 (2013).
[8] C. H. Kwon, S.-H. Lee, Y.-B. Choi, J. A. Lee, S. H. Kim, H.-H. Kim, G. M. Spinks, G. G. Wallace, M. D. Lima, M. E. Kozlov, R. H. Baughman, and S. J. Kim, Nat. Commun. **5**, 3928 (2014).
[9] G. Slaughter and T. Kulkarni, J. Biochip Tissue Chip **5**(1), 1000110 (2015).
[10] M. J. Cooney, V. Svoboda, C. Lau, G. Martina, and S. D. Minteer, Energy Environ. Sci. **1**, 320 (2008).
[11] A. Zebda, C. Gondran, A. L. Goff, M. Holzinger, P. Cinquin, and S. Cosnier, Nat. Commun. **2**, 370 (2011).
[12] K. So, S. Kawai, Y. Hamano, Y. Kitazumi, O. Shirai, M. Hibi, J. Ogawa, and K. Kano, Phys. Chem. Chem. Phys. **16**(10), 4823 (2014).
[13] O. Yehezkeli, R. Tel-Vered, S. Raichlin, and I. Willner, ACS Nano **5**(3), 2385 (2011).
[14] Y. Xiao, F. Patolsky, E. Katz, J. F. Hainfeld, and I. Willner, Science **299**(5614), 1877 (2003).
[15] J. T. Holland, C. Lau, S. Brozik, P. Atanassov, and S. Banta, J. Am. Chem. Soc. **133**(48), 19262 (2011).
[16] M. Holzinger, A. L. Goff, and S. Cosnier, Electrochim. Acta **82**, 179 (2012).
[17] C. H. Kwon, Y. Ko, D. Shin, S. W. Lee, and J. Cho, J. Mater. Chem. A **7**(22), 13495 (2019).
[18] D. Wen and A. Eychmüller, Small **12**(34), 4649 (2016).
[19] G. Wohlfahrt, S. Witt, J. Hendle, D. Schomburg, H. M. Kalisz, and H.-J. Hecht, Acta Crystallogr., Sect. D **55**, 969 (1999).
[20] X. Xiao, T. Siepenkoetter, P. Conghaile, D. Leech, and E. Manager, ACS Appl. Mater. Interfaces **10**(8), 7107 (2018).
[21] B. Shkodra, M. Petrelli, M. A. C. Angeli, D. Garoli, N. Nakatsuka, P. Lugli, and L. Petti, Appl. Phys. Rev. **8**, 041325 (2021).
[22] C. H. Kwon, Y. Ko, D. Shin, M. Kwon, J. Park, W. K. Bae, S. W. Lee, and J. Cho, Nat. Commun. **9**(1), 4479 (2018).
[23] Y. Ko, H. Baek, Y. Kim, M. Yoon, and J. Cho, ACS Nano **7**(1), 143 (2013).
[24] D. Nam, M. Kwon, Y. Ko, J. Huh, S. W. Lee, and J. Cho, Appl. Phys. Rev. **8**, 011405 (2021).
[25] J. Zhang, X. Huang, L. Zhang, Y. Si, S. Guo, H. Su, and J. Liu, Sustainable Energy Fuels **4**(1), 68 (2020).
[26] T. Siepenkoetter, U. Salaj-Kosla, X. Xiao, S. Belochapkine, and E. Magner, Electroanalysis **28**(10), 2415 (2016).
[27] T. Siepenkoetter, U. Salaj-Kosla, X. Xiao, P. O. Conghaile, M. Pita, R. Ludwig, and E. Magner, ChemPlusChem **82**(4), 553 (2017).
[28] G. Decher, Science **277**(5330), 1232 (1997).
[29] F. Caruso, R. A. Caruso, and H. Möhwald, Science **282**(5391), 1111 (1998).
[30] M. Brust, M. Walker, D. Bethell, D. J. Schiffrin, and R. Whyman, J. Chem. Soc. **7**(7), 801 (1994).
[31] S. Sun, Adv. Mater. **18**(4), 393 (2006).
[32] J. Hernández, J. Solla-Gullón, E. Herrero, A. Aldaz, and J. M. Feliu, J. Phys. Chem. C **111**(38), 14078 (2007).
[33] X. Ren, Q. Lv, L. Liu, B. Liu, Y. Wang, A. Liu, and G. Wu, Sustainable Energy Fuels **4**(1), 15 (2020).
[34] M. Liu, R. Zhang, and W. Chen, Chem. Rev. **114**(10), 5117 (2014).
[35] Y. Ko, Y. Kim, H. Baek, and J. Cho, ACS Nano **5**(12), 9918 (2011).
[36] J. Choi and M. F. Rubner, Macromolecules **38**(1), 116 (2005).
[37] M. Zhao, Y. Gao, J. Sun, and F. Gao, Anal. Chem. **87**(5), 2615 (2015).
[38] Y. Yu, Z. Chen, S. He, B. Zhang, X. Li, and M. Yao, Biosens. Bioelectron. **52**, 147 (2014).
[39] C. Cai and J. Chen, Anal. Biochem. **332**(1), 75 (2004).
[40] M. Frasconi, A. Heyman, I. Medalsy, D. Porath, F. Mazzei, and O. Shoseyov, Langmuir **27**(20), 12606 (2011).
[41] J. Hindmarsh, Electrical Machines and Their Applications, Biocatalyst in Non-Conventional Media, 4th ed. (Pergamon Press, 1984).
[42] E. Laviron, J. Electroanal. Chem. **101**(1), 19 (1979).
[43] W. Jia, G. Valdés-Ramírez, A. J. Bandodkar, J. R. Windmiller, and J. Wang, Angew. Chem., Int. Ed. **52**(28), 7233 (2013).
[44] I. Jeerapan, J. R. Sempionatto, A. Pavinatto, J.-M. You, and J. Wang, J. Mater. Chem. A **4**(47), 18342 (2016).
[45] A. J. Bandodkar, I. Jeerapan, J.-M. You, R. Nuñez-Flores, and J. Wang, Nano Lett. **16**(1), 721 (2016).
[46] S. Yin, Z. Jin, and T. Miyake, Biosens. Bioelectron. **141**, 111471 (2019).

[47]Y. Ogawa, Y. Takai, Y. Kato, H. Kai, T. Miyake, and M. Nishizawa, Biosens. Bioelectron. **74**, 947 (2015).

[48]W. Jia, X. Wang, S. Imani, A. J. Bandodkar, J. Ramírez, P. P. Mercier, and J. Wang, J. Mater. Chem. A **2**(43), 18184 (2014).

[49]D. I. Gittins and F. Caruso, Angew. Chem., Int. Ed. **40**(16), 3001 (2001).

[50]S. Chen, K. Huang, and J. A. Stearns, Chem. Mater. **12**(2), 540 (2000).

[51]D. A. Buttry, *Advanced in Electroanalytical Chemistry: Applications of the QCM to Electrochemistry* (Marcel Dekker Inc., New York, 1991).

[52]A. J. Bard and L. R. Faulkner, *Electrochemical Methods: Fundamentals and Applications*, 2nd ed. (John Wiley & Sons, New York, 2001).